39. R. Prins, J. F. Reinders, *J. Am. Chem. Soc.* **91**, 4929–4931 (1969).
40. J. S. Miller, J. H. Zhang, W. M. Reiff, *Inorg. Chem.* **26**, 600–608 (1987).
41. W. M. Reiff, *J. Appl. Phys.* **63**, 2957–2961 (1988).
42. T. A. Albright, J. K. Burdett, M.-H. Whangbo, *Orbital Interactions in Chemistry* (Wiley, 1985).

ACKNOWLEDGMENTS

Supported by Free University Berlin, Fonds der Chemischen Industrie, Deutsche Forschungsgemeinschaft (GRK 1582, Fluorine as a Key Element), and Friedrich-Alexander-University of Erlangen-Nürnberg. We thank J. Telser and E. Bill for helpful discussions and E. Zolnhofer for synthesis and magnetochemical characterization of [Cp_2Cr]. Computing time was made available by High-Performance Computing at ZEDAT/Free University Berlin. All crystal structures have been deposited with the Cambridge Crystallographic Data Centre under accession numbers CCDC 1449790 [$C_{20}H_{30}Fe(As_2F_{11})_2{\cdot}SO_2$], CCDC 1449791 [$C_{20}H_{30}Fe(AsF_6)_2{\cdot}2HF$], CCDC 1449792 [$C_{20}H_{30}F_{14}FeRe_2$], CCDC 1449793 [$C_{20}H_{30}Fe(Sb_2F_{11})_2$], and CCDC 1449794 [$C_{20}H_{30}Fe(SbF_6)_2{\cdot}2HF$].

SUPPLEMENTARY MATERIALS

www.sciencemag.org/content/353/6300/678/suppl/DC1
Materials and Methods
Figs. S1 to S10
Tables S1 and S2
References (*43*–*53*)

7 March 2016; accepted 14 July 2016
10.1126/science.aaf6362

SOFT ELECTRONICS

Highly stretchable, transparent ionic touch panel

Chong-Chan Kim,[1]* Hyun-Hee Lee,[1]* Kyu Hwan Oh,[1,2] Jeong-Yun Sun[1,2]†

Because human-computer interactions are increasingly important, touch panels may require stretchability and biocompatibility in order to allow integration with the human body. However, most touch panels have been developed based on stiff and brittle electrodes. We demonstrate an ionic touch panel based on a polyacrylamide hydrogel containing lithium chloride salts. The panel is soft and stretchable, so it can sustain a large deformation. The panel can freely transmit light information because the hydrogel is transparent, with 98% transmittance for visible light. A surface-capacitive touch system was adopted to sense a touched position. The panel can be operated under more than 1000% areal strain without sacrificing its functionalities. Epidermal touch panel use on skin was demonstrated by writing words, playing a piano, and playing games.

Integrated touch panels provide an easy and intuitive interface for interacting with display devices. Panels have been developed with several types of sensing systems, including resistive (*1*, *2*), capacitive (*3*, *4*), surface acoustic wave (*5*), and infrared (*6*) touch. Resistive touch-sensing and capacitive touch-sensing have become common in electronic devices such as mobile phones, computers, ticketing machines, point-of-sale terminals, and information kiosks (*6*, *7*).

Both resistive and capacitive touch-sensing require transparent conducting films (TCFs). Indium tin oxide (ITO) has been mostly used owing to its sufficiently low sheet resistance (<200 ohms per square) and transparency (*8*). However, because the next generation of touch panels requires stretchability and biocompatibility to allow integration with the human body, touch panels based on ITO face issues owing to their brittle nature. Alternatives such as conducting polymers (*9*, *10*), carbon nanotubes (CNTs) (*11*, *12*), graphene (*13*, *14*), and metal nanowires (*15*, *16*) have been investigated for their combination of stretchability along with transmittance for visible light. However, the sheet resistance of these materials sharply increased when they were stretched, and these materials showed fatigue failure when repeatedly stretched (*17*). Furthermore, the biocompatibility of these alternative materials still must be demonstrated (*18*, *19*).

Hydrogels are hydrophilic polymer networks swollen with large amounts of water. Hydrogels are soft like tissue and very stretchable (*20*). Many hydrogels are biocompatible, so they can be used for drug delivery (*21*), tissue replacement (*22*), and wound healing (*23*). Some hydrogels are transparent, allowing for 99% transmittance for the full range of visible light (*24*), so they can be used to transmit optical information. Because hydrogels contain large amounts of water, which can dissolve ions, they can serve as ionic conductors. Strain sensors, pressure sensors (*25*, *26*), and actuators (*24*) have been created with hydrogels as an ionic conductor by stacking conductor/insulator/conductor layers. Thus, hydrogels can be a key ingredient for the next generation of touch panels because of their stretchability, biocompatibility, and transparency. We demonstrate an ionic touch panel using a polyacrylamide (PAAm) hydrogel containing lithium chloride (LiCl) salts.

Among the various types of touch-sensing systems, a surface-capacitive system was adopted for our ionic touch panel. In a surface-capacitive touch system, the same voltage is applied to all corners of the panel, which results in a uniform electrostatic field across the panel. When a conductor, such as a human finger, touches the panel, the touch point becomes grounded, and a potential difference is generated between the electrode and the touch point. The potential difference causes current to flow from the electrode through the finger. The magnitude of the current is determined by the distance between the touch point and electrode. As the distance decreases, a larger current is induced (*27*). This system is limited to a single touch, but it is simple in terms of structure because the panel consists of only one conductor layer and only four electrodes, with one at each corner.

The architecture of a one-dimensional (1D) ionic touch strip is shown in Fig. 1A. A strip of PAAm hydrogel containing LiCl salts (2 M) was used as an ionic conductor. The strip was connected to platinum (Pt) electrodes on both sides, and the same phase ac voltage was applied through current meters A1 and A2 to both ends. When a finger touched the strip, a closed circuit was formed because the finger was grounded, which allowed current to flow from both ends of the strip to the touch point. The signals were detected by current meters at each corner. The corresponding circuit diagram of the ionic touch strip is shown in Fig. 1B. The strip is virtually divided into two resistive parts by the touch point. Each resistor was connected with a capacitor of an electrical double layer and a current meter in series; these two parts were connected in parallel. This parallel circuit was connected in series with a capacitor created by a finger. In the parallel circuit of Fig. 1B, the effect of the capacitor that was formed by the electrical double layer was negligible because of the large capacitance of the electrical double layer and high operating frequency. The position of the touch point can be represented by a normalized distance, α. The left end and the right end of the strip correspond to $\alpha = 0$ and $\alpha = 1$, respectively.

The current flowing in two resistors can be represented by the following equations

$$I_1 \approx \frac{R_2}{R_1 + R_2} I_t = (1 - \alpha) I_t \qquad (1)$$

$$I_2 \approx \frac{R_1}{R_1 + R_2} I_t = \alpha I_t \qquad (2)$$

where I_1 and I_2 are the touching currents measured from current meters A1 and A2, respectively, and $I_t = I_1 + I_2$. The derivations of Eqs. 1 and 2 are shown in the supplement. The current change depending on the touch is shown in Fig. 1C. Baseline currents on the order of micro amperes were detected. The baseline current is a leakage current that flows through the parasitic capacitor formed between the panel and the environments (*28*). When a finger touches the gel strip, additional currents are drawn from the

[1]Department of Materials Science and Engineering, Seoul National University, Seoul 151-742, South Korea. [2]Research Institute of Advanced Materials (RIAM), Seoul National University, Seoul 151-744, South Korea.
*These authors contributed equally to this work. †Corresponding author. Email: jysun@snu.ac.kr

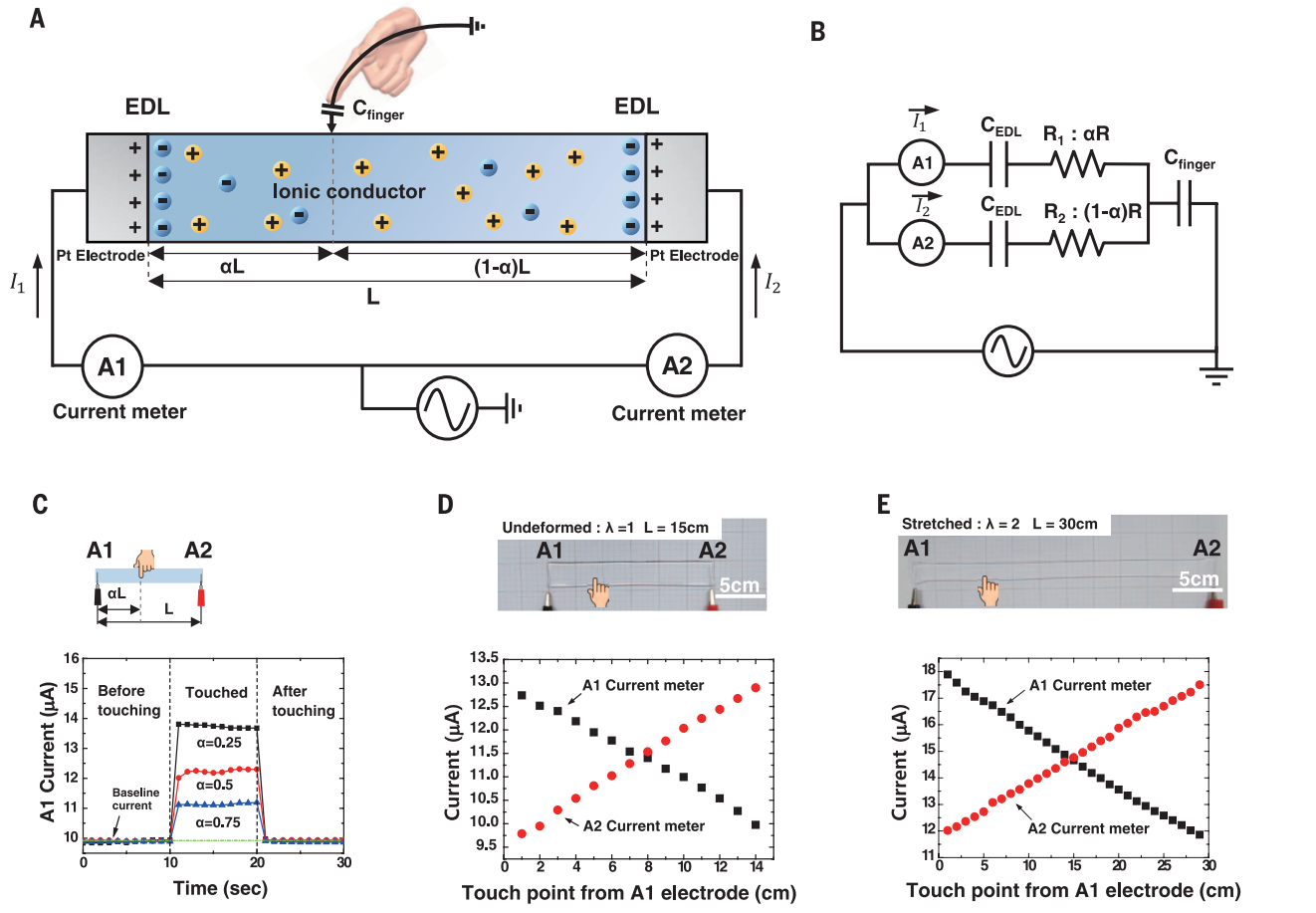

Fig. 1. A working principle of an ionic touch strip. (**A**) A schematic of a 1D ionic touch strip. When a finger touched the strip, a closed circuit was formed because the finger was grounded, which allowed current to flow from both ends of the strip to the touch point. (**B**) An electrical circuit diagram of the ionic touch strip. (**C**) The A1 current was recorded for various touch points (α = 0.25, 0.5, and 0.75). Additional touching current flowed when the strip was touched by a finger. The magnitude of the A1 current increased when the touch point became closer to the A1 electrode. The current returned to the baseline value when the strip was no longer being touched. (**D**) The average currents in a touched period were measured from A1 and A2 according to the distance from the touch point to the A1 electrode. (**E**) Linear relationship between the distance of the touch point and the current yield was maintained even after a stretching of λ = 2.

electrode to the finger (fig. S3). Here, we define this induced current as a "touching current." The latency of the touching current was <20 ms (figs. S1 and S2). The touching current was proportional to the proximity of the electrode to the touch point. The strip was touched from the left electrode to the right electrode every 1 cm, and the measured currents from the A1 current meter and A2 current meter are shown in Fig. 1D. The sum of I_1 and I_2 remained constant, and I_1 linearly decreased, whereas I_2 increased as the touch point moved to the right. The resolution of the ionic touch strip will be limited by the resolution of the current meter. With a current meter, which has a resolution in the nanoampere range, the strip showed a resolution on the order of 10^{-4} m (fig. S6). The gel strip was stretched to two times its initial length [stretch (λ) = 2, length (L) = 30 cm]. When the gel strip was stretched (Fig. 1E), the parasitic capacitance of the strip increased because of the area expansion. Thus, the baseline current and the touching current both increased compared with that of the nonstretched states. In the stretched states, the currents also showed similar negative linear correlations with the interval of the electrode and the touch points.

A 2D hydrogel panel was tested in order to detect the position of the touch point. As shown in Fig. 2, A and C, a thin hydrogel film, rectangular in shape, was connected to the Pt electrodes at each corner. Four current meters were also installed between the voltage source and each corner. Two normalized distances, α and β, were used to indicate the position of the touch on the panel. The bottom left corner of the panel corresponded to (α, β) = (0, 0), and the top right corner corresponded to (α, β) = (1, 1). When the panel is touched by a finger, it can be virtually divided into four resistive sections by the touch point (Fig. 2B). In the circuit, four virtual resistors are connected together in parallel, and this parallel circuit of resistors is connected to the capacitor by the finger in series. In Fig. 2C, the test positions of the touches are displayed. Touch points TP#1 (0.25, 0.75), TP#2 (0.75, 0.75), TP#3 (0.75, 0.25), and TP#4 (0.25, 0.25) were investigated. These points were sequentially touched, and the current changes were measured from the four current meters installed at each corner. The measured currents from each current meter are plotted in Fig. 2D. When TP#1 was touched, the closest current meter, A1, from the touch point showed the largest value, and the farthest current meter, A3, displayed the lowest value. In this 2D case, the touching current gained from the four current meters was proportional to the proximity of the electrode to the touch point, which is similar to the case of the strip. The current values could be used to calculate the coordinate of the touch points in the 2D panels.

A controller board was designed to help communication between the ionic touch panel and a computer. A block diagram of the board is shown in Fig. 2E. The board generates a drive voltage signal, and the signal is applied to the corners of the panel. The board measures the currents to each corner. The currents were on the order of a few microamperes; thus, the currents were amplified and converted to digital form in order to calculate coordinates of the touch. Because the

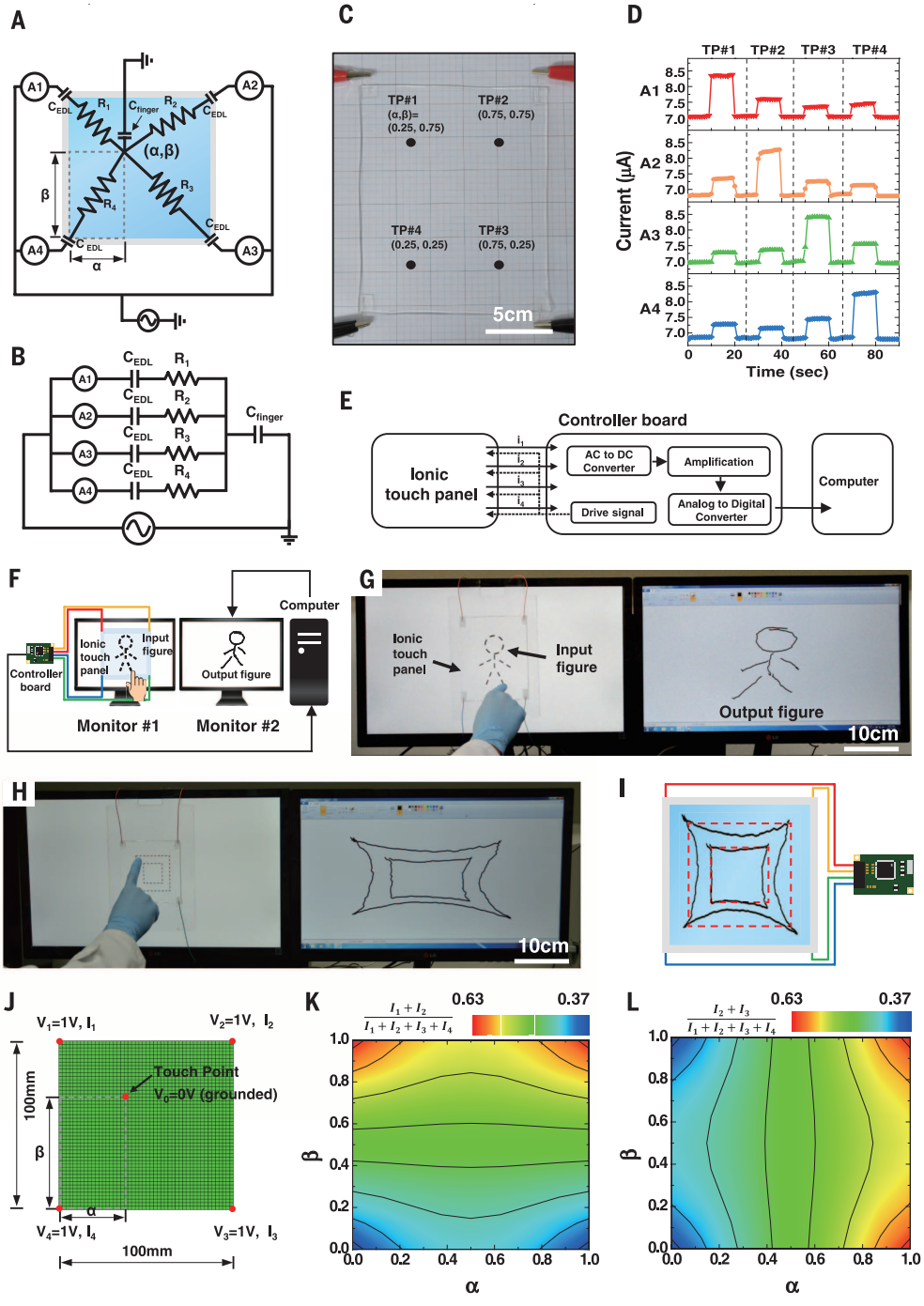

Fig. 2. Position-sensing in a 2D ionic touch panel. (**A**) A schematic diagram of an ionic touch panel. A touched position was represented by two normalized distances, α and β. (**B**) An equivalent electrical circuit of the panel during touching. (**C**) The panel was fully transparent and stable during operation. To reveal the sensitivity of position detection, four touch points (TP#1 to TP#4) of the panel were investigated. (**D**) From TP#1 to TP#4, the points were sequentially touched, and the currents measured from the four current meters were plotted against time. (**E**) A block diagram of a controller board that helps communication between the ionic touch panel and a computer. (**F** and **G**) Operation of the ionic touch panel was demonstrated with a dashed-man drawing. Monitor #1 displays the dashed man, and an ionic touch panel was attached to monitor #1. When a finger drew through the trace of the dashed man on the panel, the drawing was detected and transferred to a computer by the controller board. The output drawing was displayed on monitor #2. (**H** and **I**) The ionic touch panel showed distortion near the edges. Two concentric squares were tested on the panel, and the outer square showed more distortion than that of the inner square. (**J**) A model for a FEM simulation. The same potential of 1 V was applied to the four corners of the panel, and the touch point at its position (α, β) was grounded as boundary conditions. (**K** and **L**) We calculated $\frac{I_1+I_2}{I_1+I_2+I_3+I_4}$ and $\frac{I_2+I_3}{I_1+I_2+I_3+I_4}$ from the simulation and plotted in (K) and (L), respectively. The nonlinearity of the resistance in a 2D panel caused the distortion shown in (H).

measured currents and coordinates showed negative linear correlation, the positions were calculated based on the following equations (*27*)

$$\alpha \propto \frac{I_2 + I_3}{I_1 + I_2 + I_3 + I_4} \quad (3)$$

$$\beta \propto \frac{I_1 + I_2}{I_1 + I_2 + I_3 + I_4} \quad (4)$$

where I_1, I_2, I_3, and I_4 are increased currents by a touch measured at current meters A1, A2, A3, and A4, respectively. As shown in Fig. 2D, when a finger touches the same α coordinate, the value of Eq. 3 is determined to be the same. The β coordinate shows the same tendency as the α coordinate.

The ionic touch panel was attached to monitor #1, which displayed an input figure (Fig. 2, F and G). A 1-mm-thick polymethyl methacrylate (PMMA) plate was applied between the panel and the monitor for an electrical insulation. The panel was connected to a computer through the controller board, and the computer displayed an output figure on monitor #2 based on a signal from the controller board. We drew a man on the ionic touch panel (movie S1). Some distortion was observed on the edge of the output figures. Two concentric squares were drawn through the gel panel to test the distortion. As shown in Fig. 2, H and I, the outer square showed more distortion than the inner square. To investigate the reason for the distortion, we performed an electrical finite element method (FEM) simulation. The boundary conditions are displayed in Fig. 2J, and the electrical currents that flowed through the four corners were calculated at various touch points (α, β). A uniform electrical conductivity (1 S/m) was applied over

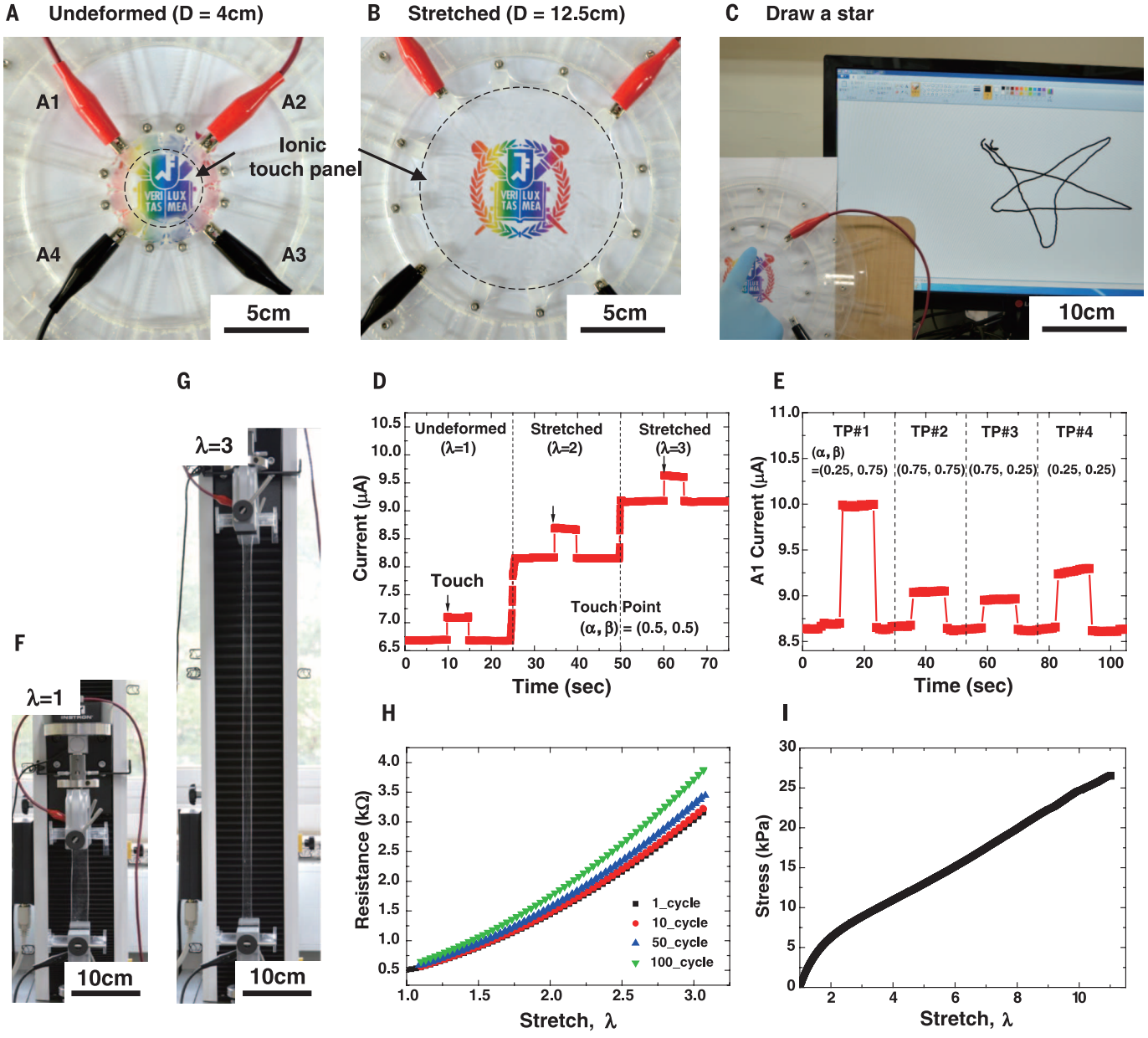

Fig. 3. A stretchable touch panel. (**A** and **B**) The ionic touch panel was stretched equibiaxially up to 1000% in area. A circular PAAm hydrogel film was glued to a biaxial stretcher, and the diameter of the hydrogel was increased from D = 4 cm to D = 12.5 cm. (**C**) The stretched touch panel was connected to a computer and operated as an input device. (**D**) The A1 current was measured before (λ = 1) and after stretching (λ = 2 and λ = 3). The baseline current increased according to the stretch of the panel. However, the touching currents were insensitive to the stretching. (**E**) The A1 current was investigated for various touch points in a stretched state (λ = 1.5). (**F** and **G**) An electromechanical test was performed on a hydrogel containing LiCl salts (2 M) up to 100 cycles. (**H**) The resistance change of the gel strip was investigated during cyclic loadings. (**I**) A uniaxial tensile test was performed on a PAAm hydrogel.

the panel, and the potential of four corners was fixed at 1 V. The panel was split into 10 grids in rows and columns. Each intersection of the grids, which is regarded as a touch point, was sequentially grounded (0 V). Plotted in Fig. 2, K and L, respectively, are $(I_1 + I_2)/(I_1 + I_2 + I_3 + I_4)$ and $(I_2 + I_3)/(I_1 + I_2 + I_3 + I_4)$ for each touch point. As shown in Fig. 2K, the contour lines near the edge of the panel were more curved than the lines near the center. Because one contour line was regarded to have the same β coordinate, the panel showed more distortion near the edge. The distortion can be reduced by carefully modifying Eqs. 3 and 4 to nonlinear equations.

We performed experiments so as to prove the stability of the touch panel in a stretched state. We prepared a circular touch panel with a diameter of 4 cm and a homemade biaxial stretcher (*24*), as shown in Fig. 3A. We glued the panel to the biaxial stretcher and connected the panel to the controller board via Pt electrodes. As shown in Fig. 3B, the diameter of the touch panel was enlarged after stretching up to 12.5 cm, which corresponded to 1000% areal strain. As shown in Fig. 3C, the touch panel can even be operated under highly stretched states. The related video clip is available in the supplementary materials (movie S2). The A1 currents of the touch panel at the undeformed and stretched states were measured with a touch point at the center in Fig. 3D. The baseline current increased from 6.68 to 9.16 μA, according to the stretch of the panel. The increase in the baseline current is suspected to be related to an expansion of the surface area of the gel panel (fig. S4), and the baseline current shows insensitivity to strain rate

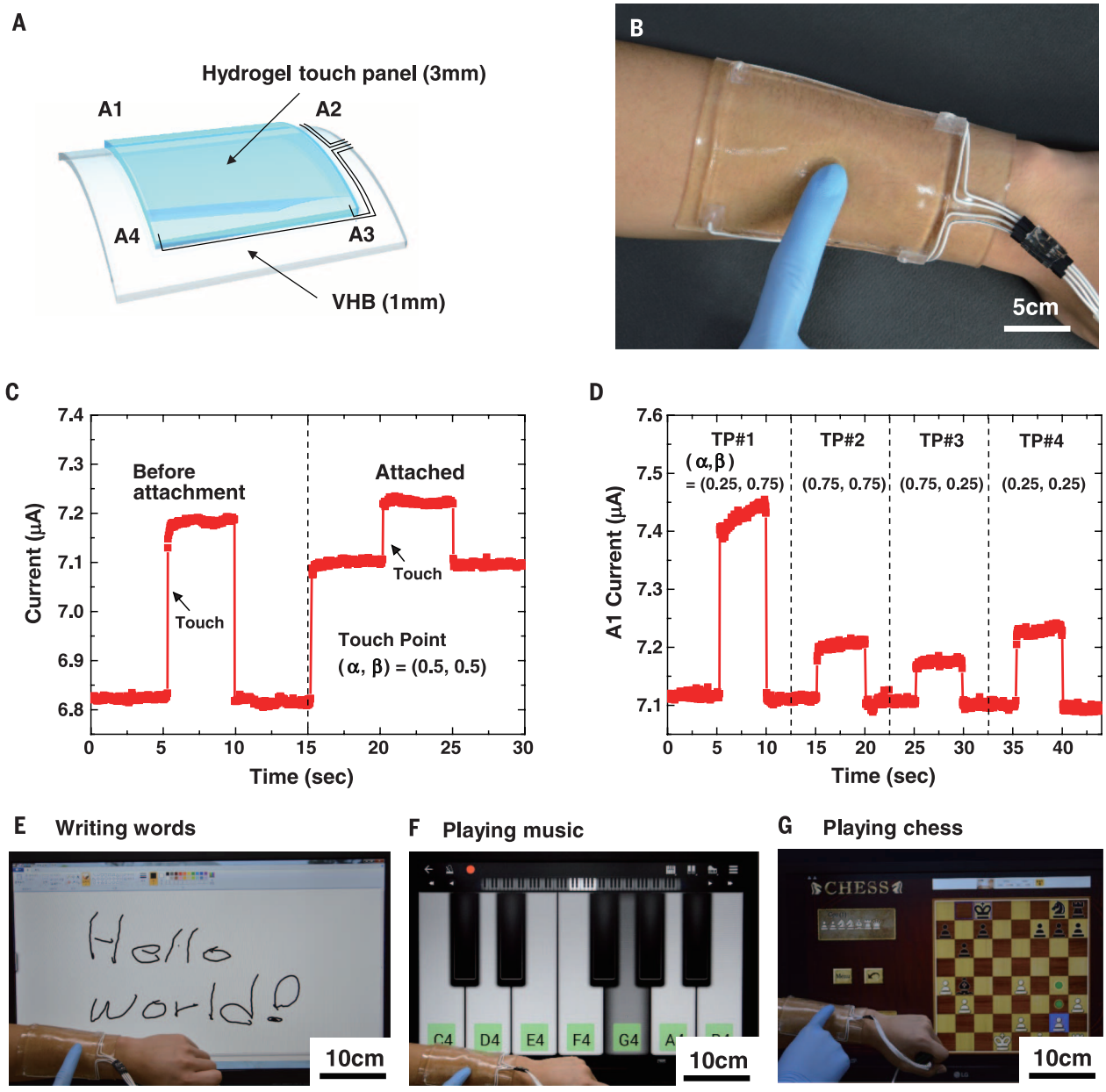

Fig. 4. An epidermal touch panel that is soft and transparent. (**A**) An epidermal touch panel was developed on a VHB substrate so as to insulate the panel from the skin and to mount the panel on a curved surface. (**B**) The touch panel was attached to an arm. (**C**) The A1 current of the panel was explored before and after attachment to an arm. (**D**) The position sensitivity after the attachment was tested by measuring the A1 currents at various touch points. (**E** to **G**) The epidermal touch panel is capable of detecting motions, such as tapping, holding, dragging, and swiping. Demonstrations such as writing words (E), playing music (F), and playing chess (G) are shown.

in the range of 0.2 to 1/min (fig. S5). When the stretched panel was touched, current was added to the baseline currents. The touching currents in a stretched state were 0.52 and 0.45 μA at λ = 2 and 3, respectively, which is similar to the current in the undeformed state (0.40 μA); the current response for a touch was not sacrificed by stretching. The current changes caused by touch during the stretching of a gel strip are shown in fig. S4. The baseline current gently increased, but the touching current was instantly increased when the strip was touched. Therefore, each current signal from stretching and touching can be distinguished by its slope as well. Four touch points were sequentially investigated with a square touch panel at a stretch of λ = 1.5, as shown in Fig. 3E. The negative correlation between distance and current was maintained in a stretched state. The panel could be operated with an anisotropic deformation. As shown in fig. S7, the output figures were slightly shifted toward the undeformed edges after the deformation. However, when we applied an additional position calibration after the deformation, the shift was compensated.

Electromechanical stability was tested for the hydrogel through a cyclic loading test up to 100 cycles (Fig. 3, F to H). The measured resistance at various cycles is presented in Fig. 3H: 1, 10, 50, and 100 cycles. The resistance slightly increased as the cycles increased, showing a maximum variation of 25% when λ = 3. We suspect that the increase in resistance during a cyclic test may originate from water evaporation in the gel. The weight of the gel decreased from 9.6 to 7.54 g after the test. A uniaxial tensile test was performed with a hydrogel specimen, as shown in Fig. 3I. The hydrogel showed an elastic modulus of 12 kPa and an elongation of λ = 11.

A schematic design of an epidermal touch panel is shown in Fig. 4A. The epidermal touch panel was built on a 1-mm-thick VHB film (3M, Maplewood, MN) so as to insulate the panel from the body. Because VHB film was originally developed as an adhesive, the panel could be attached to an arm without using extra glues (Fig. 4B). The epidermal touch panel was fully transparent so that it could convey visual content behind the touch panel. Moreover, the panel was mechanically soft and stretchable so that a user is comfortable with movement while wearing it. The currents measured before and after attachment are plotted in Fig. 4C. The baseline currents increased after the attachment owing to a leakage of charges through the VHB substrate. The thicker insulating layer generated a smaller baseline current. The effect of thickness of the insulating layers on the baseline currents is shown in fig. S8. The sensitivity to touch decreased after the attachment; however, the touching current was still sufficient to be detected. As shown in Fig. 4D, we subsequently touched from TP#1 to TP#4 on the epidermal touch panel, and the current was measured with the A1 current meter. The correlation between the measured currents and the touched position was not influenced by the attachment. The epidermal touch panel could successfully perceive various motions, such as tapping, holding, dragging, and swiping. Thus, various applications can be easily managed by integrating the panel. As shown in Fig. 4, E to G, writing words (Fig. 4E), playing music (Fig. 4F), and playing chess (Fig. 4G) were accomplished via adequate motions on the epidermal touch panel (movies S3 to S6).

We have demonstrated a highly stretchable and transparent ionic touch panel. We used a PAAm hydrogel containing 2 M LiCl salts as an ionic conductor. We investigated the mechanism of position-sensing in an ionic touch panel with a 1D strip. The ionic touch strip showed precise and fast touch-sensing, even in a highly stretched state. We expanded the position-sensing mechanism to a 2D panel. We could draw a figure using the 2D ionic touch panel. The ionic touch panel could be operated under >1000% areal strain. An epidermal touch panel was developed based on the ionic touch panel. The epidermal touch panel could be applied onto arbitrarily curved human skin, and its use was demonstrated by writing words and playing the piano and games.

REFERENCES AND NOTES

1. T. Young, U.S. patent 5,241,308 (1993).
2. R. Aguilar, G. Meijer, *Proc. IEEE Sens.* **2**, 1360–1363 (2002).
3. S. P. Hotelling, J. A. Strickon, B. Q. Huppi, U.S. patent 7,663,607 (2010).
4. P. T. Krein, R. D. Meadows, *IEEE Trans. Ind. Appl.* **26**, 529–534 (1990).
5. R. Adler, P. J. Desmares, *IEEE Trans. Ultrason. Ferroelectr. Freq. Control* **34**, 195–201 (1987).
6. M. R. Bhalla, A. V. Bhalla, *Int. J. Comput. Appl.* **6**, 12–18 (2010).
7. D. Langley *et al.*, *Nanotechnology* **24**, 452001 (2013).
8. R. Bel Hadj Tahar, T. Ban, Y. Ohya, Y. Takahashi, *J. Appl. Phys.* **83**, 2631–2645 (1998).
9. M. Vosgueritchian, D. J. Lipomi, Z. Bao, . *Adv. Funct. Mater.* **22**, 421–428 (2012).
10. Y. Xia, K. Sun, J. Ouyang, *Adv. Mater.* **24**, 2436–2440 (2012).
11. L. Hu, W. Yuan, P. Brochu, G. Gruner, Q. Pei, *Appl. Phys. Lett.* **94**, 161108 (2009).
12. Z. Wu *et al.*, *Science* **305**, 1273–1276 (2004).
13. J. Zang *et al.*, *Nat. Mater.* **12**, 321–325 (2013).
14. S. Bae *et al.*, *Nat. Nanotechnol.* **5**, 574–578 (2010).
15. L. Hu, H. S. Kim, J.-Y. Lee, P. Peumans, Y. Cui, *ACS Nano* **4**, 2955–2963 (2010).
16. S. De *et al.*, *ACS Nano* **3**, 1767–1774 (2009).
17. C. F. Guo *et al.*, *Proc. Natl. Acad. Sci. U.S.A.* **112**, 12332–12337 (2015).
18. O. Akhavan, E. Ghaderi, *ACS Nano* **4**, 5731–5736 (2010).
19. L. Ding *et al.*, *Nano Lett.* **5**, 2448–2464 (2005).
20. J.-Y. Sun *et al.*, *Nature* **489**, 133–136 (2012).
21. Y. Qiu, K. Park, *Adv. Drug Deliv. Rev.* **64**, 49–60 (2012).
22. M. C. Darnell *et al.*, *Biomaterials* **34**, 8042–8048 (2013).
23. K. Obara *et al.*, *Biomaterials* **24**, 3437–3444 (2003).
24. C. Keplinger *et al.*, *Science* **341**, 984–987 (2013).
25. J. Y. Sun, C. Keplinger, G. M. Whitesides, Z. Suo, *Adv. Mater.* **26**, 7608–7614 (2014).
26. C. Larson *et al.*, *Science* **351**, 1071–1074 (2016).
27. W. Pepper Jr., U.S. patent 4,293,734 (1981).
28. H. Haga *et al.*, *SID Symp. Dig. Tec.* **41**, 669–672 (2010).

ACKNOWLEDGMENTS

This work was supported by the National Research Foundation of Korea (NRF) grant funded by the Korean Government (MSIP) (2015R1A5A1037668). J.-Y.S. and H.-H.L. acknowledge the support of the source technology and materials funded by the Ministry of Trade, Industry and Energy of Korea (MOTIE) (10052783).

SUPPLEMENTARY MATERIALS

www.sciencemag.org/content/353/6300/682/suppl/DC1
Materials and Methods
Figs. S1 to S11
References (*29*–*31*)
Movies S1 to S6

14 April 2016; accepted 19 July 2016
10.1126/science.aaf8810

SLEEP RESEARCH

Local modulation of human brain responses by circadian rhythmicity and sleep debt

Vincenzo Muto,[1,2,3]* Mathieu Jaspar,[1,2,3]* Christelle Meyer,[1,2]* Caroline Kussé,[1,2] Sarah L. Chellappa,[1,2] Christian Degueldre,[1,2] Evelyne Balteau,[1,2] Anahita Shaffii-Le Bourdiec,[1,2] André Luxen,[1,2] Benita Middleton,[4] Simon N. Archer,[5] Christophe Phillips,[1,2,6] Fabienne Collette,[1,2,3] Gilles Vandewalle,[1,2] Derk-Jan Dijk,[5]† Pierre Maquet[1,2,7]†‡

Human performance is modulated by circadian rhythmicity and homeostatic sleep pressure. Whether and how this interaction is represented at the regional brain level has not been established. We quantified changes in brain responses to a sustained-attention task during 13 functional magnetic resonance imaging sessions scheduled across the circadian cycle, during 42 hours of wakefulness and after recovery sleep, in 33 healthy participants. Cortical responses showed significant circadian rhythmicity, the phase of which varied across brain regions. Cortical responses also significantly decreased with accrued sleep debt. Subcortical areas exhibited primarily a circadian modulation that closely followed the melatonin profile. These findings expand our understanding of the mechanisms involved in maintaining cognition during the day and its deterioration during sleep deprivation and circadian misalignment.

Forgoing sleep and staying up at night, be it for professional or recreational reasons, is highly prevalent in modern societies (*1*). Acute sleep loss leads to deterioration of multiple aspects of cognition (*2*) and is associated with increased risk of human errors and health hazards (*3*). These effects are often attributed to the mere lack of sleep. However, despite the progressive buildup of sleep pressure during wakefulness, human performance remains remarkably well preserved until wakefulness is extended into the biological night. This is attributed to a putative circadian alerting signal that increases during the day and reaches its peak in the early evening, close to the rise of melatonin concentration, to counter the mounting homeostatic sleep pressure (*4*–*6*). Cognition deteriorates rapidly and substantially when wakefulness is extended into the night and early morning hours. This is attributed to the accumulated sleep pressure and the dissipation of the circadian alerting signal (*6*, *7*). Whether and how this interaction between homeostatic sleep pressure and circadian rhythmicity is represented at the regional brain level is not known. Single–time

[1]GIGA-Cyclotron Research Centre–In Vivo Imaging, University of Liège, Liège, Belgium. [2]Walloon Excellence in Life Sciences and Biotechnology (WELBIO), Liège, Belgium. [3]Psychology and Cognitive Neuroscience Research Unit, University of Liège, Liège, Belgium. [4]Faculty of Health and Medical Sciences, University of Surrey, Guildford, UK. [5]Sleep Research Centre, Faculty of Health and Medical Sciences, University of Surrey, Guildford, UK. [6]Department of Electrical Engineering and Computer Science, University of Liège, Liège, Belgium. [7]Department of Neurology, CHU Liège, Liège, Belgium.
*These authors contributed equally to this work. †These authors contributed equally to this work. ‡**Corresponding author. Email: pmaquet@ulg.ac.be**

Editor's Summary

Soft and still responsive

Transparent touch screens, from large-panel interactive information maps to advanced cell phones, have become a part of daily life. However, such devices all use hard materials. Kim *et al.* have developed a soft touch panel based on polyacrylamide hydrogels (cross-linked polymers swollen with water) that are highly transparent and contain trapped LiCl to enhance conductivity. The hydrogels are soft and can be stretched extensively while still maintaining touch sensitivity.

Science, this issue p. 682